Results of analogue tectonic models of rifting and tectonic lineament reactivation along the Main Ethiopian Rift (https://doi.org/10.5880/fidgeo.2025.041)

Zwaan, F.[1,2,3], Muluneh, A.A.[1,4], Liu, J.[1,5], Kosari, E.[1], Rosenau, M.[1], Corti, G.[6], Sani, F.[7]

1. *GFZ Helmholtz Centre for Geosciences, Telegrafenberg, 14473 Potsdam, Germany*
2. *University of Fribourg, Department of Geosciences, Chemin du Musée 6, 1700 Fribourg, Switzerland*
3. *University of Lausanne, Institute of Earth Sciences, Géopolis, 1015 Lausanne, Switzerland*
4. *MARUM, University of Bremen, Leobener Staße 8, 28359 Bremen, Germany*
5. *Department of Earth Sciences, Freie Universität Berlin, Malteserstraße 74-100, 12249 Berlin, Germany*
6. *CNR-IGG, Consiglio Nazionale delle Ricerche, Istituto di Geoscienze e Georisorse, Via G. La Pira 4, 50121 Firenze, Italy*
7. *Università di Firenze, Dipartimento di Scienze della Terra, Via G. La Pira 4, 50121 Firenze, Italy*

1. Licence

2. Citation

When using the data please cite:

Zwaan, F., Muluneh, A.A., Liu, J., Kosari, E., Rosenau, M., Corti, G., Sani, F. (2025). Results of analogue tectonic models of rifting and tectonic lineament reactivation along the Main Ethiopian Rift. GFZ Data Services. https://doi.org/10.5880/fidgeo.2025.041

The data are supplementary material to:

Zwaan, F., Muluneh, A.A., Liu, J., Kosari, E., Rosenau, M., Corti, G., Sani, F. (2025). Local strain reorientation explains deformation of rift-oblique tectonic lineaments along the Main Ethiopian Rift. Τεκτονικα. https://doi.org/10.55575/tektonika2025.3.1.86

Table of contents

3. Data Description

This data set includes results from a total of 13 analogue tectonic models aimed at stimulating the activation of tectonic lineaments associated with the Main Ethiopian Rift in eastern Africa. We use a model set-up based on previous work by Zwaan et al. (2021, 2022). This set-up involves a velocity discontinuity (VD, i.e., the edge of a mobile base plate) to induce extension in the overlying brittle- and viscous model materials representing the upper and lower crust, respectively. Additional structural weaknesses (seeds) at the base of the brittle layer serve to represent activated tectonic weaknesses (lineaments) in nature. Model parameters (different VD and seed orientation, and different seed diameters) are summarized in Table 1. The model results presented in this data publication are obtained through Digital Image Correlation (DIC) and Structure-from-Motion (SfM) analyses. A more detailed description of model set-up, model results, and their interpretation can be found in Zwaan et al. (2025)

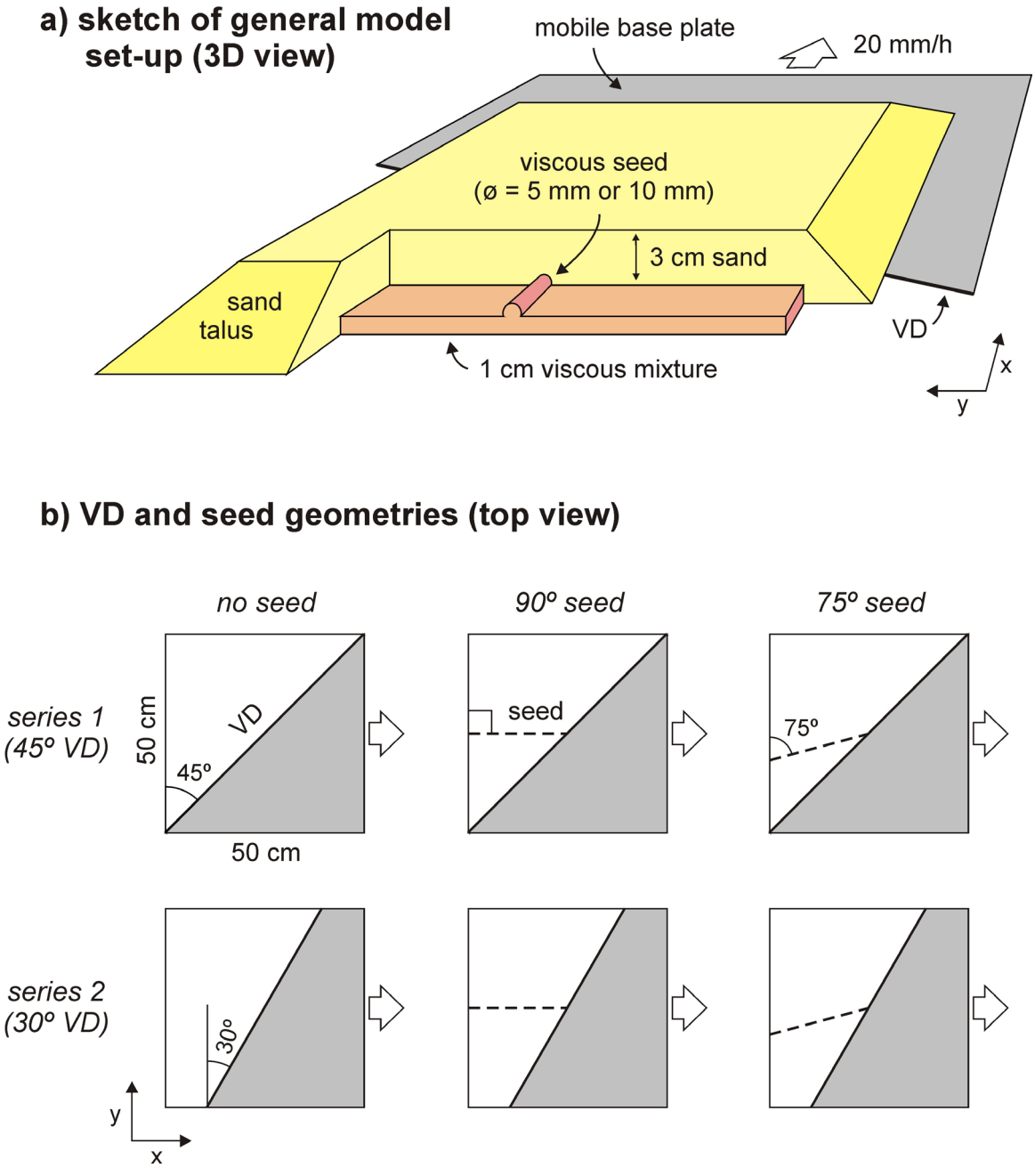

Figure 1. *Model set-up. (a) 3D sketch of model set-up and layering. (b) orientations of VD (velocity discontinuity) and seeds in the various models.*

Table 1: *Model name and parameters*

	Model lab code	Model name in Zwaan et al. (2025)	VD orientation[a]	Seed orientation[a]	Seed thickness
-	87-013[b]	R0	0˚	90˚	10 mm
Series 1	87-001	R1	45˚	-	-
	87-005	A1	45˚	90˚	5 mm
	87-006	A2	45˚	90˚	10 mm
	87-004	A3	45˚	75˚	5 mm
	87-011	A4	45˚	75˚	10 mm
Series 2	87-010	R2	30˚	-	-
	87-012	B1	30˚	90˚	5 mm
	87-009	B2	30˚	90˚	10 mm
	87-007	B3	30˚	75˚	5 mm
	87-008	B4	30˚	75˚	10 mm
Additional models	*87-002[c]*	-	*45˚*	-	-
	87-003[d]	-	*45˚*	-	-

a. See Fig. 1 for definition (VD = velocity discontinuity)
b. Additional reference model involving orthogonal rifting (VD = 0˚)
c. Rerun of Model 87-001, but Davis stopped working after ca. 36.5 mm of base plate displacement, hence all digital image correlation (DIC) data are limited to this interval. However, the Structure-from-Motion (SfM) topography data represent the end of the model run, after 50 mm of base plate displacement.
d. Benchmark model run without sand cover

4. Data presentation

Below we describe how the results in this data publication are presented. Note that the results are rotated 90˚ counter clockwise when presented in Zwaan et al. (2025). (see also the orientation used in Fig. 1). Moreover, although the total model run duration of each model is 2:30 h (representing 50 mm of base plate displacement), the analysis presented in Zwaan et al. (2025) focusses on the first 1:30 h of the model run (representing 30 mm of base plate displacement).

4.1. Digital image correlation (DIC results)

We use a digital image correlation technique (particle image velocimetry, PIV) for quantitative surface deformation monitoring (e.g., Adam et al., 2005). A stereoscopic pair of two 12-bit, 29-megapixel monochrome cameras (LaVision Imager XLite 29M) is deployed to monitor surface deformation at high spatial (8 px/mm) and temporal resolution. One image is taken every 0.5 mm of displacement. Recorded image sequences are processed by commercial PIV software LaVision Davis 10.1 to derive the surface topography and the three-dimensional surface velocity (or incremental

displacement) field, from which any component of the 3D surface incremental and cumulative strain tensor can be derived. To exclude boundary effects, we choose a central area of interest. The spatial resolution of the processed vector fields is 2 mm in terms of grid cell size and <5 µm in terms of displacement precision. For visualization and analysis of the surface deformation, we trace model topography and horizontal displacement over time. Moreover, we map the incremental horizontal maximum normal (or principal) strain as an absolute measure of strain

4.1.1. Topography evolution videos

For each model we provide a video depicting the model's topographic evolution (Fig. 2). Note that benchmark model 87-003 is without sand cover (see Table 1).

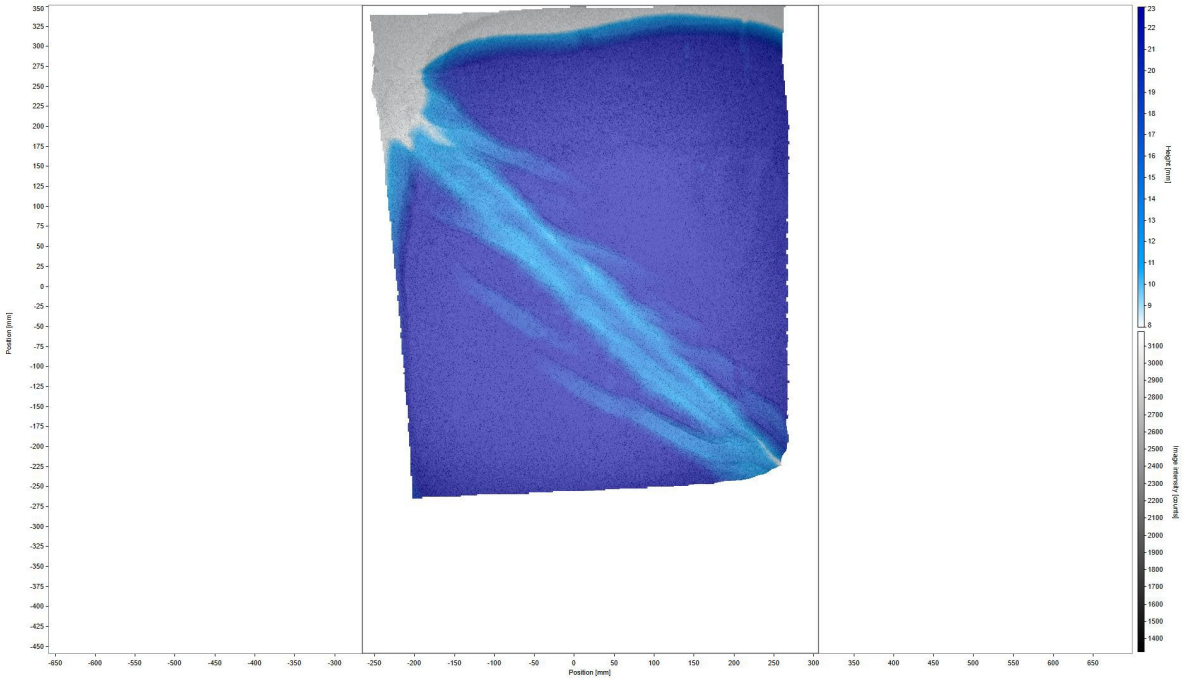

Figure 2. *Video still showing the final topography of model 87-001 (after 50 mm of base plate displacement) in map view. Topography is indicated in blues; the background is a greyscale photograph of the model surface.*

4.1.2. Maximum normal strain evolution videos

For each model (except for model 87-003) we provide a video depicting the model's incremental maximum normal strain (MNS) evolution (Fig. 3). These incremental MNS results represent the long axis of the strain ellipse and indicate active faulting over the interrogation interval (1 mm of base plate displacement). For benchmark model 87-003 (without sand cover, see Table 1) we provide a video with cumulative results.

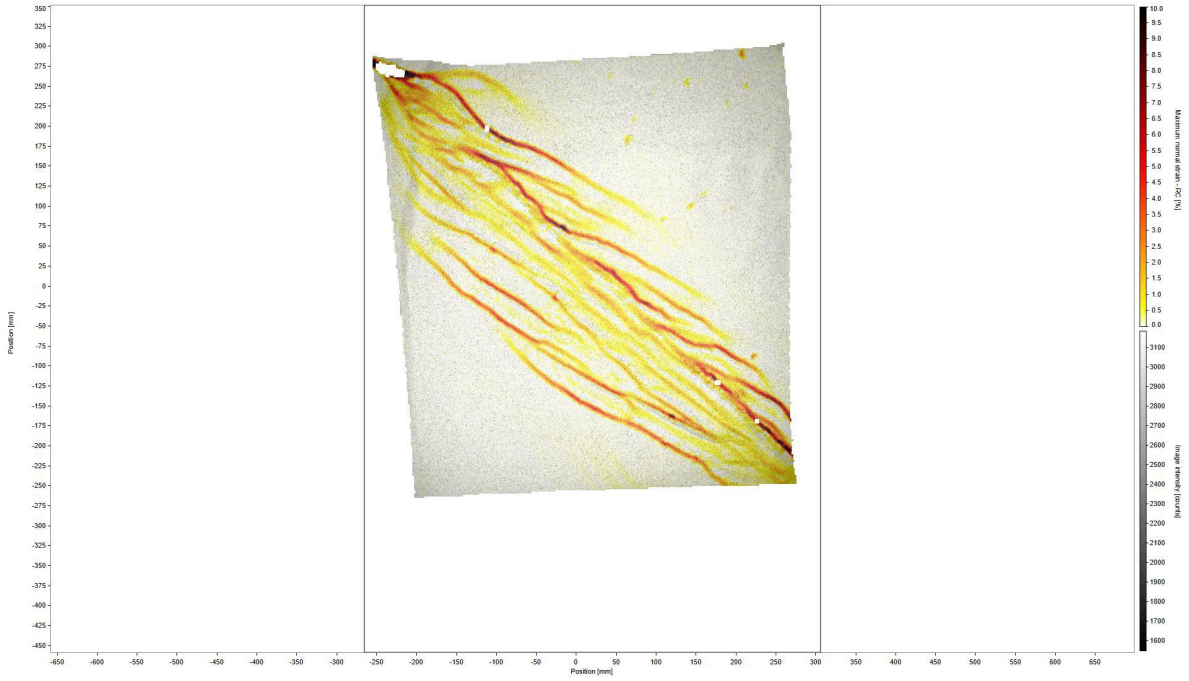

Figure 3. *Video still showing the incremental maximum normal strain (MNS) results of model 87-001 (after 50 mm of base plate displacement) in map view. MSN is indicated in yellow-red-black colours; the background is a greyscale photograph of the model surface.*

4.1.3. Horizontal displacement evolution videos

For each model (except for model 87-003) we provide a video depicting the model's incremental horizontal displacement evolution at interrogation intervals of 1 mm of base plate displacement (Fig. 4). For benchmark model 87-003 (without sand cover, see Table 1) we provide a video with cumulative results.

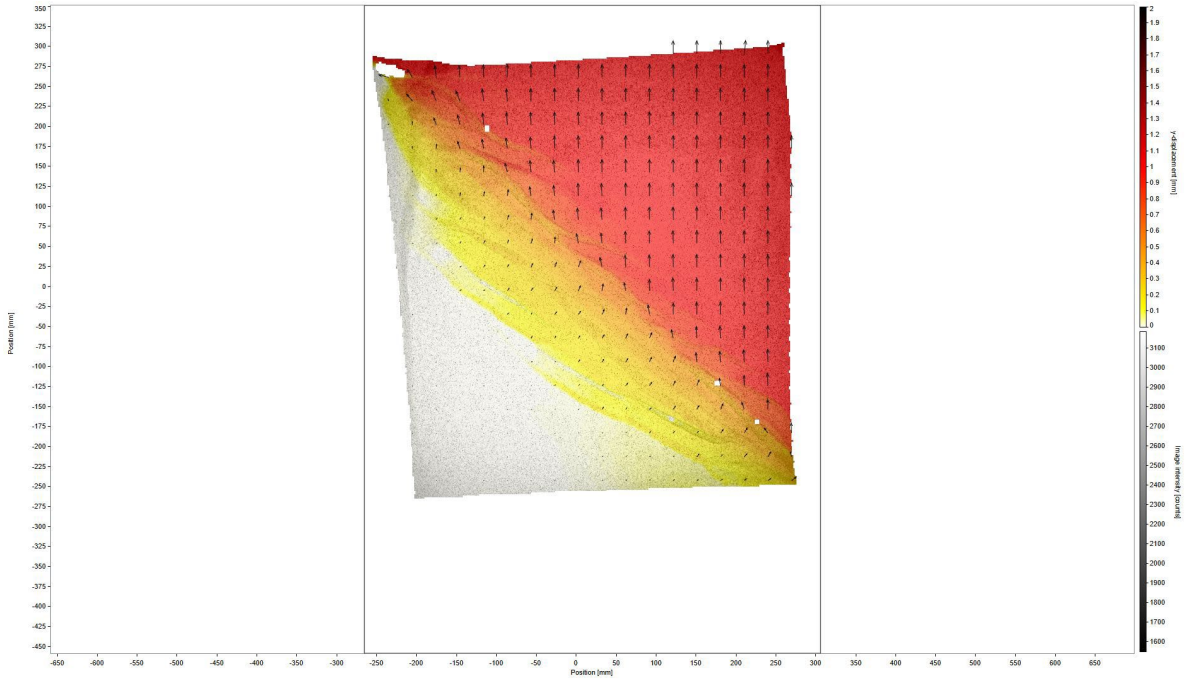

Figure 4. *Video still showing the incremental horizontal displacement evolution of model 87-001 (after 50 mm of base plate displacement) in map view. Red-yellow-black colours indicate horizontal displacement in the y-direction, the vectors indicate general displacement. The background is a greyscale photograph of the model surface.*

4.2. Final model topography obtained with Structure-from-Motion analysis

For each model (except for models 87-003 and 87-013) we provide a high-resolution reconstruction of the model's surface topography, as well as of the topography of the viscous layer below (Fig. 5), at the end of the model run (after 50 mm of base plate displacement). The photogrammetric technique we apply, termed 'Structure-from-Motion' (SfM) (e.g., Westoby et al., 2012), is deployed to acquire high-resolution digital elevation models (DEM) at an intermediate (25%) and finite state (50% extension), respectively. We use a consumer-grade digital camera (Canon D810) to take overlapping top- and oblique-view photographs on the surface. These photographs were inputted into the software Agisoft Photoscan (Metashape) to produce a 3-D point cloud and, finally, a DEM with a high resolution of 0.24 mm/pixel.

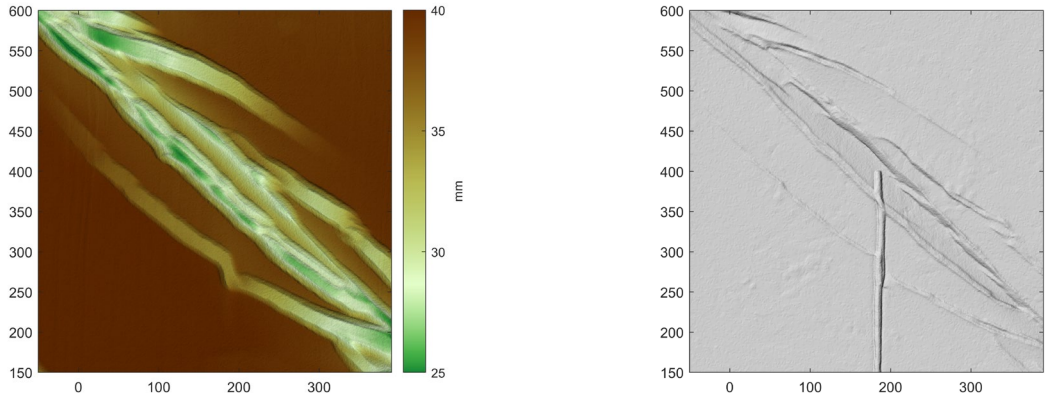

Figure 5. *Examples of high-resolution topography reconstructions of the model's surface (left) or the top of the top of the viscous layer (right). Imagery from model 87-005.*

5. File description

For each of the 13 models the following data are provided:

i. Video of model topography evolution (.mp4 format)
ii. Video of model maximum normal strain evolution (.mp4 format)
iii. Video of model horizontal displacement evolution (.mp4 format)

Moreover, for all models except 87-003 and 87-013, we provide the following data:

- Final model topography reconstruction (.tif and .jpg formats)

An overview of all files of the data set is given in the **List of Files.**

6. Acknowledgements

We thank Frank Neumann and Thomas Ziegenhagen for technical assistance in the lab, , Uwe Lemgo for IT support, and Kirsten Elger for helping us prepare this data publication. Frank Zwaan received financial support in the form of a GFZ Discovery Fellowship and an Equality Grant from by the Faculty of Geosciences and Environment at the University of Lausanne. Ameha Muluneh was funded by German Research Foundation (DFG, 537025018), Jun Liu received financial support from the China Scholarship Council (CSC NO. 202006190038).

7. References

Adam, J., Urai, J. L., Wieneke, B., Oncken, O., Pfeiffer, K., Kukowski, N., Lohrmann, J., Hoth, S., Van der Zee, W., Schmatz, J. (2005). Shear localisation and strain distribution during tectonic faulting—new insights from granular-flow experiments and high-resolution optical image correlation techniques. Journal of Structural Geology, 27, 283-301. https://doi.org/10.1016/j.jsg.2004.08.008

Westoby, M.J., Brasington, J., Glasser, N.F., Hambray, M.J., Reynolds, J.M. (2012). 'Structure-from-Motion' photogrammetry: A low-cost, effective tool for geoscience applications. Geomorphology 179, 300-314. https://doi.org/10.1016/j.geomorph.2012.08.021

Zwaan, F., Chenin, P., Erratt, D., Manatschal, G., Schreurs, G. (2021). Complex rift patterns, a result of interacting crustal and mantle weaknesses, or multiphase rifting? Insights from analogue models. Solid Earth, 12, 1473-1495. https://doi.org/10.5194/se-12-1473-2021

Zwaan, F., Chenin, P., Erratt, D., Manatschal, G., Schreurs, G. (2022). Competition between 3D structural inheritance and kinematics during rifting: Insights from analogue models. Basin Research, 34, 824-854. https://doi.org/10.1111/bre.12642

Zwaan, F., Muluneh, A.A., Liu, J., Kosari, E., Rosenau, M., Corti, G., Sani, F. (2025). Local strain reorientation explains deformation of rift-oblique tectonic lineaments along the Main Ethiopian Rift. Τεκτονικα. https://doi.org/10.55575/tektonika2025.3.1.86